Abid Muhammad Adnan (Orcid ID: 0000-0002-7389-7977)

Ashfaq Moetasim (Orcid ID: 0000-0003-4106-3027)

Kucharski Fred (Orcid ID: 0000-0002-8710-8051)

Evans Katherine, J. (Orcid ID: 0000-0001-8174-6450)

Tropical Indian Ocean Mediates ENSO Influence Over Central Southwest Asia During the Wet Season

Muhammad Adnan Abid[1,2], Moetasim Ashfaq[3], Fred Kucharski[1,2], Katherine J. Evans[3], Mansour Almazroui[2]

[1]*Earth System Physics, The Abdus Salam International Centre for Theoretical Physics (ICTP), Trieste, Italy*

[2]*Centre of Excellence for Climate Change Research (CECCR)/Department of Meteorology, King Abdulaziz University, Jeddah, Saudi Arabia*

[3]*Computational Sciences and Engineering Division, Oak Ridge National Laboratory, Oak Ridge, Tennessee, United States*

Geophysical Research Letters

Corresponding Author:
M. Adnan Abid
Earth System Physics, The Abdus Salam International Centre for Theoretical Physics, I-34151, Trieste, Italy
(email: mabid@ictp.it)
ORCID: https://orcid.org/0000-0002-7389-7977

Key Points:

- ENSO influence on the CSWA wet season precipitation variability varies intra-seasonally
- Diabatic heating anomalies in the Tropical Indian Ocean play major role in the mediation of ENSO-CSWA teleconnection
- Atmospheric response to diabatic heating anomalies in the Tropical Indian Ocean is reproducible in a numerical model experiment

Abstract

El Niño-Southern Oscillation (ENSO) modulates wet season (November–April) precipitation over Central Southwest Asia (CSWA), however, intra-seasonal characteristics of its influence are largely unknown, which can be important for its sub-seasonal to seasonal hydroclimate predictability. Here we show that the ENSO-CSWA teleconnection varies intra-seasonally and is a combination of direct and indirect positive influences. The direct influence is through a Rossby wave-like pattern in the tail months. The indirect influence is through an atmospheric dipole of diabatic heating anomalies in the tropical Indian Ocean (TIO) as a result of ENSO-forced response, which also generates a Rossby wave-like forcing and persists throughout the wet season. ENSO exerts its strongest influence when both direct and indirect modes are in phase, while the relationship breaks down when the two modes are out of phase. The atmospheric teleconnection through the atmospheric diabatic heating anomalies in the TIO is reproducible in numerical simulations.

Plain Language Summary

El Niño-Southern Oscillation (ENSO) exerts a strong positive influence on the precipitation variability over Central Southwest Asian (CSWA) region during the wet season that spans from November to April. We note that the ENSO influence varies intra-seasonally and has two components, one directly through the equatorial Pacific region and one indirectly through the tropical Indian Ocean. In both cases, ENSO exerts its influence through Rossby wave-like atmospheric anomalies. When the two components are in phase, ENSO has the strongest influence while it is weakest when they are out of phase. These findings suggest that improvements in sub-seasonal to seasonal scale predictability requires the better representation of intra-seasonal variability of ENSO teleconnection, as well as the role of inter-basin interactions in its propagation.

1. Introduction

Central Southwest Asia (CSWA) is home to a widespread heterogenous climate, ranging from the largest glaciers outside of the polar regions in the northeast to the Arabian desert in the southwest. Freshwater in the region largely depends on the precipitation received during highly variable wet season that stretches from November to April. Most of the precipitation comes through the mid-latitude storms, also known as Western Disturbances (WD), that transport moisture from the Mediterranean Sea, the Atlantic Ocean, and other terrestrial and oceanic sources (Barlow et al., 2016; Dimri, 2013; Dimri et al., 2015; Hunt et al., 2018; Kamil et al., 2019; Syed et al., 2010; Syed et al., 2006). The movement of WDs to the region is aided by the presence of a Subtropical Westerly Jet (SWJ), which persists throughout the wet season (Hoell et al., 2013). The interannual variability of wet season precipitation over the region is strongly linked to the remote influence of the El Niño-Southern Oscillation (ENSO), with a generally positive (negative) anomaly during its warm (cold) phase (Abid et al., 2016; Barlow et al., 2002; Hoell et al., 2015; Kamil et al., 2019; Kang et al., 2015; Mariotti, 2007; Rana et al., 2018; Yadav et al., 2010; Yu et al., 2018).

ENSO establishes its influence over remote regions through stationary Rossby waves that propagate from the equatorial Pacific to the higher latitudes (e.g. Wallace and Gutzler, 1981). Additionally, it can exert its influence through anomalies in inter-basin interactions between the Pacific Ocean and other oceanic basins (e.g. Cai et al., 2019). In the case of the CSWA region, the ENSO-driven Rossby wave forcing during the warm phase establishes an upper-level trough over the region, which causes a southward shift in the storm tracks, favoring more precipitation during the wet season (Abid et al., 2016; Kang et al., 2015). Furthermore, earlier studies also suggest an enhanced moisture transport from the Indian Ocean towards CSWA during the warm phase of ENSO (Cannon et al., 2017; Hoell et al., 2015; Mariotti, 2007), which points towards the ENSO influence through inter-basin interactions. The tropical

oceans, such as the Indian and Pacific Oceans, are connected via Walker circulations in the atmosphere. ENSO induces changes in the Walker circulation that favors reduced precipitation over the western Pacific and eastern Indian Ocean and enhanced precipitation over the western Indian Ocean. Studies also relate the development of the Indian Ocean Dipole (IOD; (Saji et al., 1999)) to ENSO forcing, with positive (negative) sea surface temperatures (SSTs) anomalies in the western (eastern) Indian Ocean (e.g. Stuecker et al., 2017). While the IOD mainly peaks in autumn, well before the start of wet season over the CSWA, the precipitation dipole in the tropical Indian Ocean (TIO) has been shown to persist throughout the CSWA wet season and is independent of the classical IOD (e.g. Molteni et al., 2015). This precipitation dipole, which we will refer to as the Tropical Western-Eastern Indian Ocean dipole (hereafter TWEIO), has the potential to propagate the ENSO influence to remote regions, such as CSWA, by inducing changes in the atmospheric circulations through atmospheric diabatic heating anomalies (e.g. Barlow et al., 2007; Wilson et al., 2013). However, to our knowledge, a systematic evaluation of ENSO induced diabatic heating anomalies over the Indian Ocean, such as the TWEIO, and their role in the ENSO teleconnection to remote regions, such as CSWA, has not yet been explored. Moreover, with the exception of a few (e.g. Hoell et al., 2018), most of the studies that investigate the ENSO-CSWA teleconnection thus far have focused on their relationship at seasonal scales (Kamil et al., 2019; Kang et al., 2015; Yadav et al., 2010; Rana et al., 2018) and a gap exists in our understanding towards its intra-seasonal characteristics.

The understanding towards the ENSO-CSWA teleconnections at intra-seasonal scales is of value for sub-seasonal to seasonal (S2S) predictability. The reliability of the seasonal prediction skill for the wet season precipitation over the CSWA is still a challenge, which spatiotemporally varies across different seasonal forecast modeling systems depending on their ability in representing the ENSO SSTs variability and their remote influence on the CSWA

precipitation (Ehsan et al., 2020; Abid et al., 2016; Shirvani and Landman, 2016). Given the high seasonality and strong inter-annual variability of precipitation over the CSWA region, improvements in precipitation predictions are highly desired at S2S timescale. However, the requirements for improving the prediction skills in the seasonal forecasting systems may not be limited to the reproducibility of seasonal ENSO teleconnections, as it may also require the representation of its intra-seasonal characteristics, and inter-basin linkages to other tropical oceans. To this end, the understanding towards the existence of the ENSO-forced TWEIO pattern during the CSWA wet season motivates the investigation of its potential role in the propagation of ENSO teleconnection at intra-seasonal timescales.

Therefore, in this study, we focus on the intra-seasonal precipitation variability during the CSWA wet season in association with its ENSO teleconnection, with a focus on the potential role of the TWEIO. We first establish our understanding through the analyses of relevant variables from a reanalysis data and subsequently use a set of numerical model experiments to support our findings.

2. Methods

We obtain SSTs, precipitation, geopotential height (GPH), specific humidity, mean sea level pressure, and atmospheric winds from the fifth generation of the European Reanalysis (ERA5) data at a 0.25°×0.25° horizontal grid spacing and at an hourly timescale for 1981-2018 (C3S, 2017), which are regridded to 1°×1° horizontal grid and temporally averaged to generate monthly means.

We use multiple standardized precipitation indices over three different regions for analyses, including the ENSO region, the TIO, and the CSWA region. We define the ENSO forcing using the Niño3.4 monthly precipitation index, which is area-averaged over the central-eastern equatorial Pacific region between 190–240°E and 5°S–5°N. It is pertinent to mention that Niño3.4 precipitation is a proxy for the SSTs in the region, as SSTs variability in the ENSO

region is known to force precipitation anomalies of similar nature (Curtis and Adler, 2000; Molteni et al., 2015). The consistency between the global teleconnections of ENSO forcing using SSTs and that using precipitation over the Niño3.4 has also been demonstrated in Figure S1. The precipitation index over the TIO represents the TWEIO region, which is based on the area-averages over the tropical western (40–80°E; 10°S–10°N) and eastern (90–140°E; 10°S–10°N) Indian Ocean (Molteni et al., 2015). The CSWA precipitation index is defined as the area-average over 45–80°E and 22–40°N.

Additionally, using the intermediate complexity International Centre for Theoretical Physics (ICTP) Atmospheric Global Climate Model (AGCM), named "SPEEDY" (Molteni, 2003; Kucharski et al., 2006; Kucharski et al., 2013) [https://www.ictp.it/research/esp/models/speedy.aspx], we investigate the sensitivity of the large scale atmospheric CSWA circulation response to the atmospheric heating anomalies in the TIO. Further details regarding model and experiments can be found in the *Supplementary Material*.

3. Results and Discussion

3.1 CSWA wet season precipitation variability

We regress monthly anomalies of the global precipitation, 200-hPa GPH (Z200), and 200-hPa velocity potential (VP; CHI200) onto the area-averaged CSWA standardized precipitation index (Fig. 1) for each month during the wet season. The regression with the global precipitation anomalies identifies those regions that may have potential influence on the CSWA precipitation variability. On the other hand, the regressions with the GPH and VP fields reveal the overlying atmospheric mechanisms that establish a causative relationship of the CSWA precipitation with some of those regions beyond the correlative associations identified in the precipitation maps. Consistent with wet season mean precipitation (Fig. S2), the regression with global precipitation anomalies reveals two local maxima over CSWA region,

one covering the western Himalayan and Hindukush, and one covering the Northeast Arabian Peninsula. Moreover, the CSWA precipitation exhibits significant but intra-seasonal varying associations with tropical oceans, including the Niño3.4 region, and the TIO. The relationship of the CSWA precipitation with Niño3.4 is generally positive in all months except for January and February (Fig. 1c–d). However, a statistical significant relationship with Niño3.4 only exists in November. In January, the relationship reverses with Niño4, while it stays positive with Niño3. In February, the positive relationship with Niño3.4 reverses to weak negative and interestingly reappears during late season (Fig. 1e–f). The regression also reveals a significant association between CSWA precipitation and the TIO. During early part of the wet season (November and December), a precipitation dipole appears in the TIO, with positive anomalies in the west and negative anomalies in the east, which represents the TWEIO region. The positive side of the dipole in the western Indian Ocean slightly weakens in January, completely reverses in February, and partially reappears during the late season. Irrespective of the sign, the spatial fluctuations in the anomaly pattern in the western Indian Ocean can be partly due to seasonal changes in the spatial distribution of precipitation (Fig. S2).

When the 200-hPa GPH anomalies are regressed onto the CSWA standardized precipitation index, a Rossby wave-like pattern emerges with positive anomalies over the central and eastern Pacific region and negative anomalies over the CSWA where the SWJ is located during the wet season (Fig. 1g–l). Such anomalies in the SWJ increase the influence of WDs over the CSWA region, resulting in a precipitation surplus (Abid et al., 2016; Dimri et al., 2015). While the anomalous upper-level trough over CSWA mostly persists during the wet season, the pattern of positive anomalies over the Pacific Ocean varies intra-seasonally with substantial weakening during January and February, consistent with the intra-seasonal variability shown in the precipitation regression maps. In the VP regression maps (Fig. 1m–r), an anomalous significant upper-level convergence is present over the eastern Indian and

western Pacific Oceans (the warm pool region), which is compensated by two anomalous intra-seasonally varying upper-level divergent centers. The first center is over west Asia, Africa and western Indian Ocean which is statistically significant at 95% level. The second relatively weak and mostly insignificant center is over the central-eastern Pacific (i.e., Niño3.4 region), pointing to its weaker connection with the CSWA precipitation. The anomalous divergence over Niño3.4 region starts subsiding in January and mostly reverses in February, which is consistent with the precipitation maps in Figure 1c–d. It should be noted that the background upper-level flow is divergent over the warm pool region and convergent over the eastern Pacific and western Indian Oceans, which represents the Walker circulation branches in the Pacific and Indian Oceans (Fig. S3). The anomaly patterns in the VP reflect a weakening of these two Walker circulation branches, which is generally similar to a typical ENSO-forced pattern (e.g. Cai et al., 2019).

Overall, these analyses suggest a potential influence of ENSO on the variability of CSWA wet season precipitation, as it has been reported in several earlier studies. However, there exists a substantial monthly variation that conceivably points towards the intra-seasonal variability in the CSWA-ENSO teleconnection. Therefore, in order to disentangle the forcing mechanisms responsible for the intra-seasonal variations in the CSWA precipitation, we start with the influence of ENSO on the monthly CSWA precipitation in the next section.

3.2 Direct influence of ENSO on the monthly CSWA precipitation

The ENSO-forced teleconnections at the global scale can be manifested by regressing monthly global precipitation onto the standardized Niño3.4 precipitation index (Fig. 2a–f). Several regions exhibit a persistent relationship with ENSO throughout the wet season, including parts of North America and southeast China (Fig. 2a–f). A significant positive relationship is noted between Niño3.4 region and the CSWA precipitation in November, which reduces to weak positive in December and during the late season. However, it seemingly

diminishes during the mid-season (i.e., January and February; Fig. 2c–d), which is consistent with the intra-seasonal variations noted in Figure 1. ENSO also forces a dipole like precipitation anomaly (TWEIO) over the TIO, which exhibits spatial variations intra-seasonally (Fig. 2a–f). While part of these spatial fluctuations in the precipitation anomalies are due to the spatial variability of precipitation over the Indian Ocean (Fig. S2), there are conspicuously consistent similarities between these spatial variations and the fluctuation in the ENSO-CSWA relationship, which point towards a potential role of the TWEIO in the propagation of the ENSO forcing over the CSWA region.

We further explore the atmospheric processes that regulate the ENSO-CSWA relationship by regressing monthly Niño3.4 precipitation anomalies onto the 200-hPa GPH and VP anomalies (Fig. 2g–l). Expectedly, a Rossby wave-like pattern emerges in the GPH regressions that propagate the ENSO influence towards the higher latitudes. While this pattern bears similarities to Figure 1g–l, there are also sharp disparities, in particularly, during the mid-season where our analyses points towards a breakdown in the ENSO-CSWA relationship. During January and February (Fig. 2i–j), a positive height anomaly appears over western Russia that stretches southwards over the Arabian Peninsula, which reduces the strength of the SWJ and causes a mixed and insignificant precipitation response over CSWA (Fig. 2c–d). Additionally, we note that the upper level trough over CSWA is not significant during the late season (Fig. 2k–l). The comparison between the VP regression in Figures 1(m-r) and 2 (m-r) further corroborates the fact that the strength of the CSWA-ENSO relationship varies intra-seasonally as there is a good correspondence in November and December but sharp contrasts in the rest of the months.

3.3 Indirect influence of ENSO via TIO on the monthly CSWA precipitation

Given that there is an indication of the role of the TIO in the propagation of the ENSO influence over the CSWA region, we regress monthly global precipitation anomalies onto the

standardized TWEIO precipitation index (Fig. S4a–f). There is a positive relationship between the TWEIO and CSWA precipitation (Fig. S4a–f), similar to the Figure 1a–f, which is not only stronger than the Niño3.4-forced CSWA precipitation anomalies (Fig. 2a–f) but is also present in all months including January when the Niño3.4 and CSWA relationship is absent. Additionally, we note that this relationship is statistically significant over most of the CSWA region in all months except for February. Furthermore, a strong positive relationship appears with the ENSO region consistent to that noted in Figures 1 and 2 (a-f). The strength of the TWEIO precipitation dipole varies within the wet season, where relatively weaker positive anomalies are noted in February (Fig. S4d).

We explain the association of the TWEIO with the CSWA precipitation by regressing the monthly 200-hPa GPH and VP anomalies onto the corresponding standardized TWEIO precipitation index (Fig. S4g–r). The GPH regression patterns over the CSWA region for November and December generally match with Figure 1 and 2. However, the correspondence of upper-level trough in terms of its strength and statistical significance is high between the TWEIO and CSWA precipitation-based maps. Nonetheless, the resemblances in all three cases during the early season provide evidence that ENSO establishes its positive teleconnection with the CSWA region both directly through Rossby wave-like response and indirectly through the TWEIO. Figure S1 shows that TWEIO covaries with the Niño3.4 SST index. Clearly, a correlation or co-variance does not imply a cause-effect relationship in one or the other direction. There are several studies showing that the Indian Ocean can trigger ENSO but with several months delay (Izumo et al., 2010; 2014). Thus, the contemporaneous covariation suggests that the TWEIO signal is forced by ENSO. Interestingly, the TWEIO forcing also produces a strengthened SWJ in January (Fig. S4i) and to some extent in February (Fig. S4j), similar to the ones seen in Figure 1i–j, opposite to the Niño3.4 regression maps (Fig. 2i–j), which potentially suggest that the positive influence of ENSO on the CSWA precipitation only

propagates through the TIO during the mid-season. The more dominant role of the TWEIO in the propagation of ENSO teleconnection is also evident in the late season (March and April) where GPH regression patterns over the CSWA closely match between Figures 1 and S4 (k–l). Similarly, the regression of the VP anomalies (Fig. S4 m–r) produces a pattern of divergent wind anomalies over the western Indian Ocean and the CSWA region similar to the one seen in Figure 1m–r throughout the season, which are largely absent in the corresponding regressions with Niño3.4 (Fig. 2m–r). The only exception exists in February when the anomalous divergent winds center over the western Indian Ocean and the CSWA region is largely absent.

Our analyses thus far provide ample evidence that ENSO exhibits a varying influence on the precipitation variability over the CSWA region. Furthermore, our analyses reveal that the role of the TIO persists throughout the wet season, which becomes more prominent during the middle of the wet season. In order to separate the direct and indirect influences of ENSO on the CSWA precipitation, we make use of partial regression, which is discussed in the next section.

3.4 Separation of direct and indirect influences of ENSO the CSWA precipitation variability

We make use of a partial regression (see *Supplementary* text) to separate out the direct and indirect influences of ENSO on the CSWA precipitation variability. The relationships of the CSWA precipitation with the ENSO and TWEIO indices as a coupled system, as well as linearly independent from each other, are shown in Figure 3a–b. The Niño3.4 relationship with CSWA is statistically significant in November and weak positive in December and April. On the other hand, the TWEIO relationship with CSWA is not only stronger than Niño3.4, it is statistically significant in all months except in February. When the effects of Niño3.4 and the TWEIO are removed from each other, the positive relationship between the CSWA and Niño3.4 is reduced in November and April, while the correlations become negative during the

rest of the season. Contrarily, the TWEIO relationship with CSWA not only remains consistent in all months, but it gets even stronger in January and February – the two months where the Niño3.4 relationship with CSWA is minimal without the removal of the TWEIO. These analyses point to the fact that apart from November and April, ENSO does not exert direct positive influence on the CSWA precipitation and throughout the wet season its influence is propagated through the TIO.

We further elaborate the direct and indirect influences of ENSO on the CSWA precipitation by regressing the 200-hPa GPH (shown as contours) and global precipitation anomalies (shown as shaded) onto the linearly independent TWEIO and Niño3.4 precipitation indices (Fig. 3c-h). With the removal of the direct ENSO influence, the upper-level circulation anomalies in Figure 3c–h are cyclonic (dotted lines) over the CSWA region, which should favor more precipitation – a finding consistent with our earlier analysis (Fig. 1). Moreover, after the removal of direct ENSO influence (Niño3.4), TWEIO also triggers a favorable thermodynamic response in the form of enhanced moisture flux from the Indian Ocean towards the CSWA region that persists throughout the wet season (Fig. S5). Conversely, with the removal of the indirect ENSO influence (TWEIO), the upper-level circulation anomalies in Figure 3i–n are mostly anticyclonic (solid lines) over the CSWA region in all months except for November and April. The anticyclonic anomalies favor less precipitation, which is consistent with our earlier analysis (Fig.2). The removal of the TWEIO also reduces the moisture flux from TIO towards the CSWA region (Fig. S5), which, combined with the unfavorable dynamic anomalies in the atmosphere, weakens the indirect ENSO influence and disrupts the ENSO-CSWA connection in all months where the ENSO teleconnection with CSWA is primarily through the TIO.

3.5 Robustness of TIO role as a mediator

In order to establish the robustness of the TIO role as a mediator in the ENSO-CSWA teleconnection, which has been noted in our statistical analyses, we force an AGCM with a dipole of atmospheric diabatic heating anomalies over the TIO with positive anomalies in the west and negative anomalies in the east, which represents the latent heating anomalies induced by the ENSO-forced TWEIO precipitation. The details of experimental design are provided in the *Supplementary* text.

The difference between the experiments with and without the TWEIO-like diabatic heating anomalies in the atmosphere suggests that the TWEIO generates a sub-tropical Rossby wave-like response in the SPEEDY model (Fig. 4). The generated wave pattern is structurally similar to the one seen in Figure 3c–h. The GPH anomaly patterns exhibit an upper level trough over the western and central parts of west Asia, which supports enhanced precipitation over the CSWA region. The reproducibility of reanalysis-based circulation anomalies in the numerical model experiment confirms the presence of indirect influence of ENSO through the TIO. We also note that these findings are not sensitive to the choice of the dataset. For consistency, the precipitation in our analyses is from ERA5 as spatiotemporal distribution of anomalies in the reanalysis-based atmospheric circulations and observations-based precipitation do not always align (Mukherjee et al., 2020). However, results shown are largely unchanged if we replace ERA5 precipitation with the observed precipitation, such as Global Precipitation Climatology Project (Adler et al., 2018) (Fig. S6). Likewise, similar results can be reproduced with the use of National Center for Environmental Prediction/National Center for Atmospheric Research reanalysis (Kalnay et al., 1996)(Fig. S7).

4. Summary

In the present study, we revisit the ENSO-CSWA teleconnection at intra-seasonal timescale during the wet season. While ENSO exhibits a positive relationship with the wet season CSWA precipitation at a seasonal timescale, our analysis reveals a variable nature of

this teleconnection at a monthly scale. We note that ENSO establishes its influence directly through a Rossby wave-like pattern and indirectly through the TIO. The influence through the TIO is established via atmospheric heating anomalies, which are a result of the ENSO-forced response. Without the ENSO influence through the TIO, the ENSO-CSWA positive relationship is only limited to the tail months of the wet season. The atmospheric heating anomalies in the TIO in the shape of the TWEIO can also generate a Rossby wave-like pattern with an upper-level trough over the CSWA region, favoring a positive precipitation response. When the direct and indirect teleconnections of ENSO are in phase, ENSO exhibits the highest positive correlation with the CSWA precipitation. Alternatively, when the direct and indirect teleconnections of ENSO are out of phase, such as in the mid-season, ENSO relationship with the CSWA precipitation breaks down. The atmospheric teleconnection of TWEIO with the large-scale CSWA circulation is reproducible in a numerical model when TWEIO-like atmospheric heating anomalies are introduced in the TIO, which establishes the robustness of our findings.

The results presented in this study provide a new insight towards the intra-seasonal characteristics of CSWA precipitation relationship with ENSO within the context of inter-basin connections, which can be used as a new metric for the evaluation of seasonal forecast systems. It also highlights the fact that the path towards the prediction of sub-seasonal extremes requires a thorough understanding of the interactions across spatiotemporal scales that potentially dictate limits of regional scale predictability (Mariotti et al., 2018). Lastly, these findings warrant future research into the role of other phenomenon, such as MJO, that exert influence on the intra-seasonal precipitation variability over the CSWA (e.g. Cannon et al., 2017) and have the potential to influence ENSO-forced inter-basin interactions.

5. Acknowledgments

M. A. A. would like to acknowledge Earth System Physics Section of ICTP and Centre of Excellence for Climate Change Research (CECCR) for their support. M. A. and K. J. E. are supported by the United States Air Force Numerical Weather Modeling Program. M.A. A. would also like to thank KAU high performance computing center (https://hpc.kau.edu.sa) for providing AZIZ supercomputer resources. We also thank the two anonymous reviewers for their insightful comments.

We obtained ERA5 reanalysis from https://cds.climate.copernicus.eu/, GPCP precipitation from https://psl.noaa.gov/data/gridded/data.gpcp.html, and NCEP/NCAR reanalysis from https://psl.noaa.gov/data/gridded/. The details regarding the SPEEDY model are available at https://www.ictp.it/research/esp/models/speedy.aspx. The SPEEDY model experiment data, used in this study, are available at http://clima-dods.ictp.it/Users/mabid/GRL_Abidetal/. This manuscript has been co-authored by employees of Oak Ridge National Laboratory, managed by UT Battelle, LLC, under contract DE-AC05-00OR22725 with the U.S. Department of Energy. The publisher, by accepting the article for publication, acknowledges that the United States Government retains a non-exclusive, paid-up, irrevocable, world-wide license to publish or reproduce the published form of this manuscript, or allow others to do so, for United States Government purposes. The Department of Energy will provide public access to these results of federally sponsored research in accordance with the DOE Public Access Plan (http://energy.gov/downloads/doe-public-access-plan).

References

Abid, M. A., et al.
(2016), Interannual rainfall variability and ECMWF-Sys4-based predictability over the Arabian Peninsula winter monsoon region. *Quarterly Journal of the Royal Meteorological Society,* 142(694), 233-242.

Adler, R. F., et al.
(2018), The Global Precipitation Climatology Project (GPCP) Monthly Analysis (New Version 2.3) and a Review of 2017 Global Precipitation. *Atmosphere,* 9, 138.

Barlow, M., Cullen H., & Lyon, B.
(2002), Drought in central and southwest Asia: La Nina, the warm pool, and Indian Ocean precipitation. *Journal of Climate,* 15(7), 697-700.

Barlow, M., Hoell, A. & Colby, F.
(2007), Examining the wintertime response to tropical convection over the Indian Ocean by modifying convective heating in a full atmospheric model. *Geophysical Research Letters,* 34, L19702. doi:10.1029/2007GL030043.

Barlow, M., et al.
(2016), A Review of Drought in the Middle East and Southwest Asia. *Journal of Climate,* 29(23), 8547-8574.

C3S, Copernicus Climate Change Service
(2017), ERA5: Fifth generation of ECMWF atmospheric reanalyses of the global climate. C.C.C.S.C.D.S. (CDS), ed.

Cai, W. J., et al.
(2019), Pantropical climate interactions. *Science,* 363(6430), 944-+.

Cannon, F., et al.
(2017), The influence of tropical forcing on extreme winter precipitation in the western Himalaya. *Climate Dynamics,* 48, 1213-1232.

Curtis, S.,& Adler, R.
(2000), ENSO indices based on patterns of satellite-derived precipitation. *Journal of Climate,* 13(15), 2786-2793.

Dimri, A. P.
(2013), Relationship between ENSO phases with Northwest India winter precipitation. *International Journal of Climatology,* 33(8), 1917-1923.

Dimri, A. P., et al.
(2015), Western Disturbances: A review. *Reviews of Geophysics,* 53(2), 225-246.

Ehsan, M. A., Kucharski F., & Almazroui, M.
(2020), Potential predictability of boreal winter precipitation over central-southwest Asia in the North American multi-model ensemble. *Climate Dynamics,* 54, 473-490.

Hoell, A., Cannon, F., & Barlow, M.
(2018), Middle East and Southwest Asia Daily Precipitation Characteristics Associated with the Madden-Julian Oscillation during Boreal Winter. *Journal of Climate,* 31(21), 8843-8860.

Hoell, A., Barlow, M., & Saini, R.
(2013), Intraseasonal and Seasonal-to-Interannual Indian Ocean Convection and Hemispheric Teleconnections. *Journal of Climate,* 26(22), 8850-8867.

Hoell, A., et al.

(2015), The Forcing of Monthly Precipitation Variability over Southwest Asia during the Boreal Cold Season. *Journal of Climate,* 28(18), 7038-7056.

Hunt, K. M. R., Turner, A. G., & Shaffrey, L. C.

(2018), The evolution, seasonality and impacts of western disturbances. *Quarterly Journal of the Royal Meteorological Society,* 144(710), 278-290.

Kalnay, E., et al.

(1996), The NCEP/NCAR 40-year reanalysis project. *Bulletin of the American Meteorological Society,* 77(3), 437-471.

Kamil, S., et al.

(2019), Long-term ENSO relationship to precipitation and storm frequency over western Himalaya-Karakoram-Hindukush region during the winter season. *Climate Dynamics,* 53, 5265-5278.

Kang, I. S., et al.

(2015), Multidecadal Changes in the Relationship between ENSO and Wet-Season Precipitation in the Arabian Peninsula. *Journal of Climate,* 28(12), 4743-4752.

Kucharski, F., Molteni, F., & Bracco, A.

(2006), Decadal interactions between the western tropical Pacific and the North Atlantic Oscillation. *Climate Dynamics,* 26(1), 79-91.

Kucharski, F., et al.

(2013), On the Need of Intermediate Complexity General Circulation Models: A "SPEEDY" Example. *Bulletin of the American Meteorological Society,* 94(1), 25-30.

Mariotti, A.

(2007), How ENSO impacts precipitation in southwest central Asia. *Geophysical Research Letters,* 34, L16706. doi: 10.1029/2007GL030078.

Mariotti, A., P. Ruti, M., & Rixen, M.

(2018), Progress in subseasonal to seasonal prediction through a joint weather and climate community effort. *npj Climate and Atmospheric Science,* 1, 4. https://doi.org/10.1038/s41612-018-0014-z.

Molteni, F.

(2003), Atmospheric simulations using a GCM with simplified physical parameterization. I. Model climatology and variability in multi-decadal experiments. *Climate Dynamics,* 20, 175-191.

Molteni, F., Stockdale, T. N., & Vitart, F.

(2015), Understanding and modelling extra-tropical teleconnections with the Indo-Pacific region during the northern winter. *Climate Dynamics,* 45, 3119-3140.

Mukherjee, S., Ashfaq, M., & Mishra, A. K.

(2020), Compound Drought and Heatwaves at a Global Scale: The Role of Natural Climate Variability- Associated Synoptic Patterns and Land-Surface Energy Budget Anomalies. *Journal of Geophysical Research-Atmsospheres,* https://doi.org/10.1029/2019JD031943.

Rana, S., et al.

(2018), Seasonal Prediction of Winter Precipitation Anomalies over Central Southwest Asia: A Canonical Correlation Analysis Approach. *Journal of Climate,* 31(2), 727-741.

Saji, N. H., et al.

(1999), A dipole mode in the tropical Indian Ocean. *Nature,* 401(6751), 360-363.

Shirvani, A., & Landman, W. A.

(2016), Seasonal Precipitation forecast skill over Iran. *International Journal of Climatology*, 36, 1887-1900.

Stuecker, M. F., et al.
(2017), Revisiting ENSO/Indian Ocean Dipole phase relationships. *Geophysical Research Letters,* 44, 2481-2492. doi:10.1002/2016GL072308.

Syed, F. S., et al.
(2010), Regional climate model simulation of winter climate over Central-Southwest Asia, with emphasis on NAO and ENSO effects. *International Journal of Climatology,* 30(2), 220-235.

Syed, F. S., et al.
(2006), Effect of remote forcings on the winter precipitation of central southwest Asia part 1: observations. *Theoretical and Applied Climatology,* 86, 147-160.

Wallace, J. M., & Gutzler, D. S.
(1981) Teleconnections in the Geopotential Height Field during the Northern Hemisphere Winter. *Monthly Weather Review,* 109(4), 784-812.

Wilson, E. A., Gordon, A. L., & Kim, D.
(2013), Observations of the Madden Julian Oscillation during Indian Ocean Dipole events. *Journal of Geophysical Research-Atmospheres,* 118(6), 2588-2599.

Yadav, R. K., et al.
(2010), Why Is ENSO Influencing Northwest India Winter Precipitation in Recent Decades? *Journal of Climate,* 23(8), 1979-1993.

Yu, E. T., et al.
(2018), Asian droughts in the last millennium: a search for robust impacts of Pacific Ocean surface temperature variabilities. *Climate Dynamics,* 50, 4671-4689.

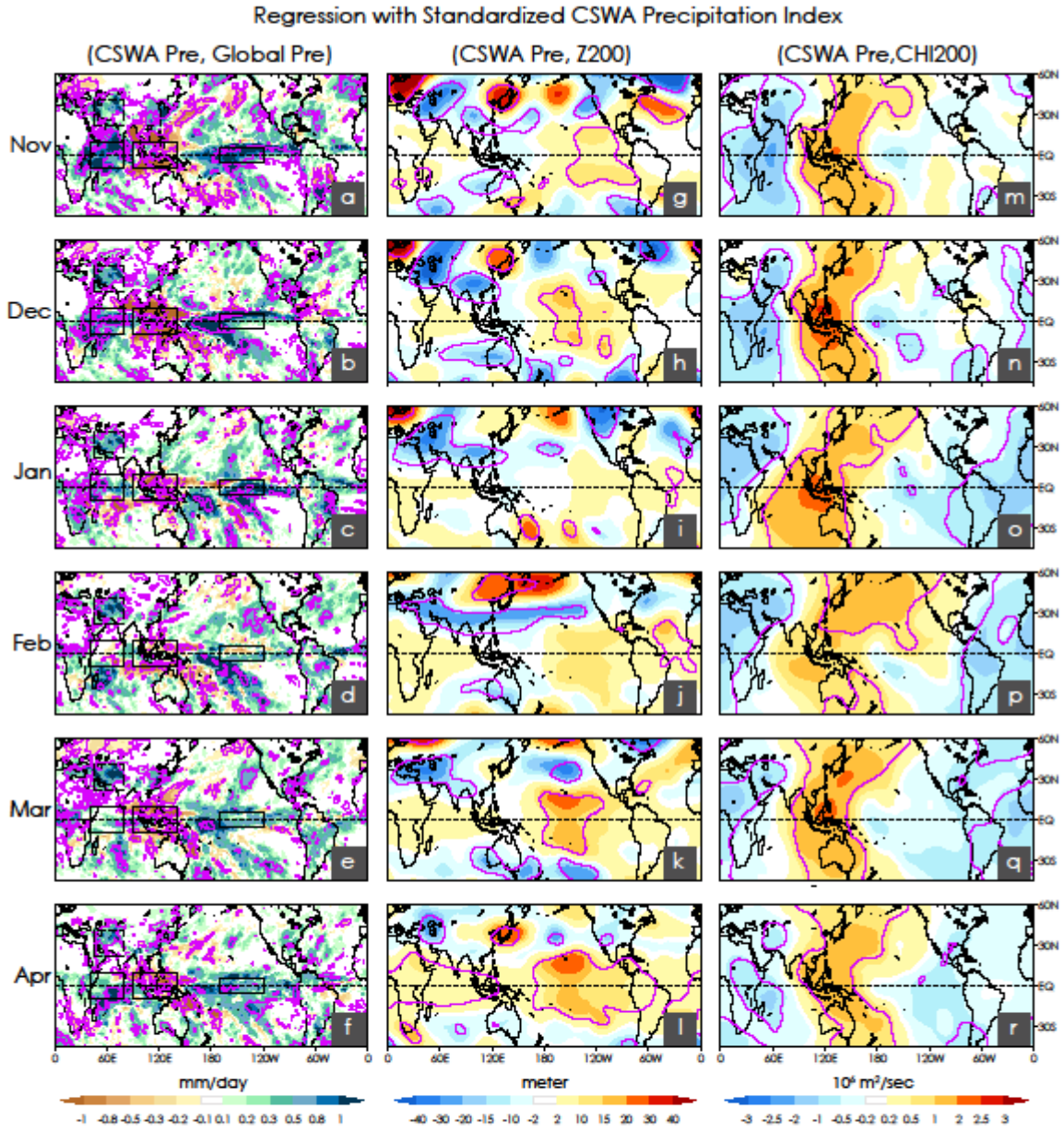

Figure 1. a-f) Regression of the monthly global precipitation anomalies onto the standardized CSWA precipitation index [45°E–80°E; 22°N–40°N] during the wet season (1981–2018; mm/day); g-l) same as in (a-f) but for the 200-hPa geopotential height (Z200) anomalies (meter); m-r) same as in (a-f) but for the velocity potential (CHI200) anomalies (10^6 m^2/sec). Purple contours represent statistical significance at 95% confidence level.

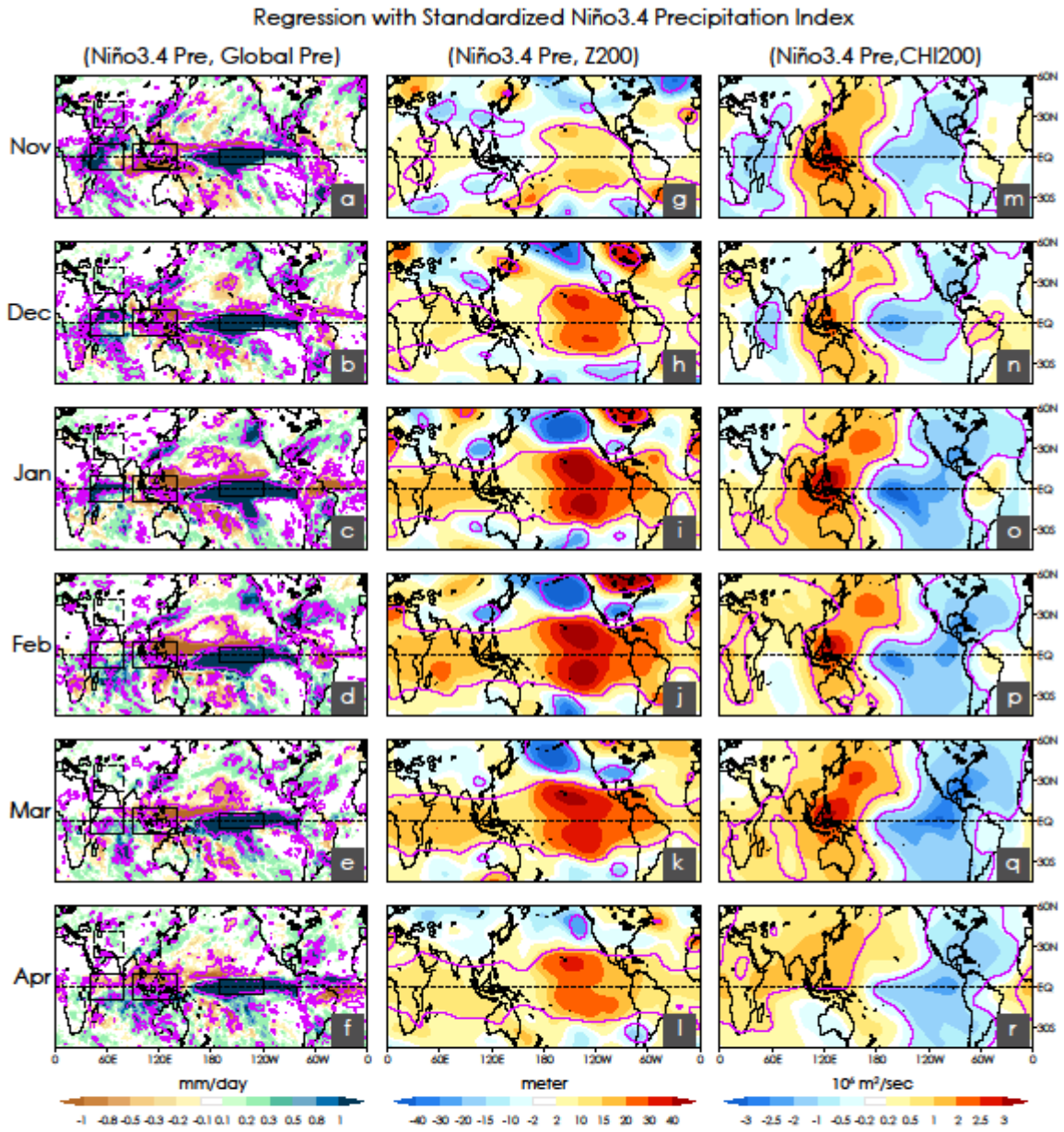

Figure 2. a-f) Same as in Figure 1 but for the standardized Niño3.4 precipitation index [190°E–240°E; 5°S–5°N].

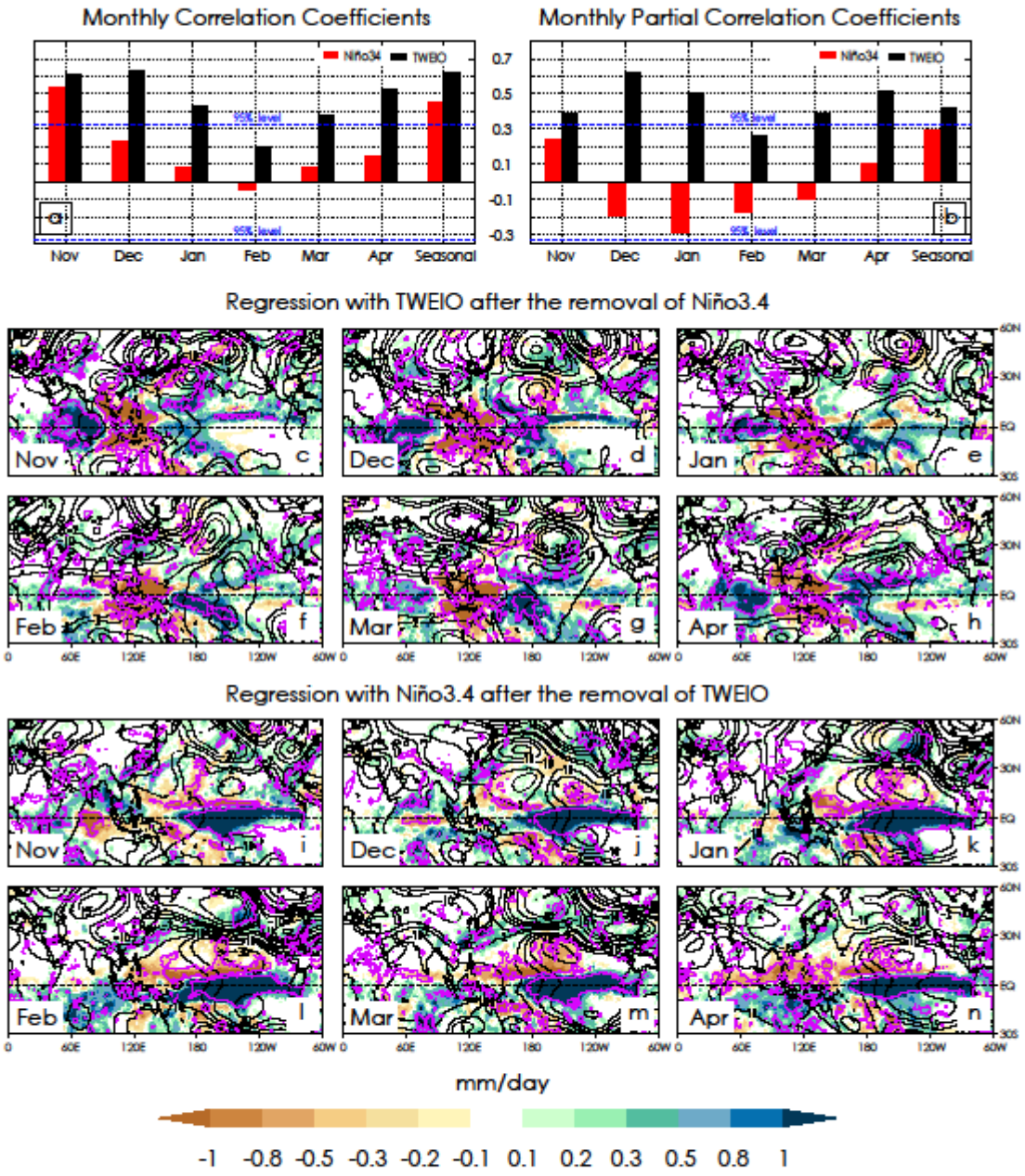

Figure 3. a) Correlations between the standardized CSWA, Niño3.4 and TWEIO precipitation indices, b) same as of (a) but with linearly independent Niño3.4 and TWEIO indices c-h) Regression of precipitation (shaded; mm/day) and 200-hPa geopotential height (Z200) anomalies (contours; meter) onto standardized TWEIO precipitation index after removing the effect of Niño3.4, i-n) same as in (c-h) but for the standardized Niño3.4 precipitation index after removing the effect of TWEIO. Purple contours represent statistical significance at 95% confidence level.

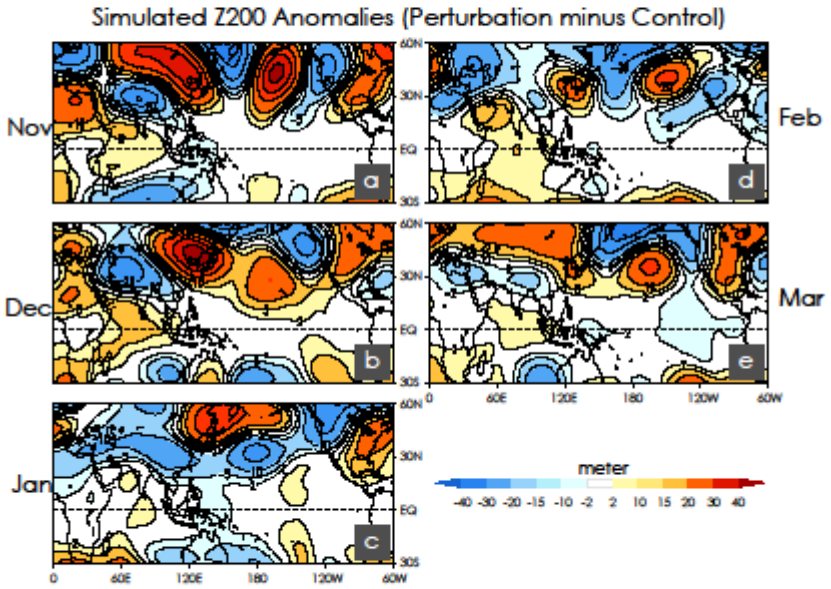

Figure 4. Difference (Perturbed minus Control) between the SPEEDY model simulation with and without perturbation, which represents heating anomalies over the tropical Indian Ocean. a-e) 200-hPa geopotential height anomalies (meter).